Molecular Structure of Membrane Tethers

Baoukina, Svetlana; Marrink, Siewert J.; Tieleman, D. Peter

Published in:
Biophysical Journal

DOI:
10.1016/j.bpj.2012.03.048

Publication date:
2012

Molecular Structure of Membrane Tethers

Svetlana Baoukina,[†‡] Siewert J. Marrink,[§¶] and D. Peter Tieleman[†‡*]
[†]Department of Biological Sciences and [‡]Institute for Biocomplexity and Informatics, University of Calgary, Calgary, Alberta, Canada; and [§]Groningen Biomolecular Sciences and Biotechnology Institute and [¶]Zernike Institute for Advanced Materials, University of Groningen, Groningen, The Netherlands

ABSTRACT Membrane tethers are nanotubes formed by a lipid bilayer. They play important functional roles in cell biology and provide an experimental window on lipid properties. Tethers have been studied extensively in experiments and described by theoretical models, but their molecular structure remains unknown due to their small diameters and dynamic nature. We used molecular dynamics simulations to obtain molecular-level insight into tether formation. Tethers were pulled from single-component lipid bilayers by application of an external force to a lipid patch along the bilayer normal or by lateral compression of a confined bilayer. Tether development under external force proceeded by viscoelastic protrusion followed by viscous lipid flow. Weak forces below a threshold value produced only a protrusion. Larger forces led to a crossover to tether elongation, which was linear at a constant force. Under lateral compression, tethers formed from undulations of unrestrained bilayer area. We characterized in detail the tether structure and its formation process, and obtained the material properties of the membrane. To our knowledge, these results provide the first molecular view of membrane tethers.

INTRODUCTION

Membrane tethers are long, thin tubes with walls constituted by lipid bilayers. They play important functional roles in eukaryotic cells and their organelles (such as the endoplasmic reticulum, mitochondria, and Golgi apparatus) (1–5). Membrane tethers are efficient structures for cellular transport and communication, as well as for storage of excess membrane area upon synthesis of new lipids or changes in cell volume (6–8). In vivo, tethers are pulled by molecular motors or induced by membrane deformation (9,10). Experimentally, tethers can be formed by application of a localized external force (e.g., using micropipette aspiration, optical or magnetic tweezers, or hydrodynamic drag) (11–16) or by compression of confined membranes (17,18). Using tether-pulling experiments in combination with theoretical models, investigators have been able to characterize a number of mechanical membrane properties (19–24) as well as lipid phase behavior (25,26). Theoretical models also can relate tether geometrical parameters to the pulling force and surface tension. However, due to the small diameters (below optical resolution) and dynamic nature of tethers, detailed structural information about tethers and their formation process is lacking.

Here we used molecular dynamics simulations to obtain molecular-level insight into the formation of tethers from model membranes. We employed the coarse-grained MARTINI model (27) to simulate lipid bilayer patches of 4608 and 18,432 dioleoylphosphatidylcholine (DOPC) molecules in water containing 500,000–3,700,000 water particles on a microsecond timescale. Large-scale simulations representing tens of millions of molecules warranted the use of a coarse-grained force field. MARTINI was previously applied successfully to simulate a wide range of lipid assemblies, including various lipid phases and their transformations, vesicle fusion, and monolayer folding (see Marrink et al. (28) for review).

METHODS

All simulations were performed with the Gromacs software package (v.4.5.4) (29). The MARTINI coarse-grained force field (27) was used. In this force field, molecules are represented by beads, each of which represents approximately four nonhydrogen atoms. DOPC is a standard component of this force field. The angle potential at particles C2 and D3 in the hydrocarbon chains was modified to an equilibrium angle of 100° and a force constant of 10 kJ/mol to better reproduce a decrease in the order parameter profile at the unsaturated bond.

We simulated two systems: a small (4608 lipids) and a large (18,432 lipids) DOPC bilayer solvated in ~500,000 and 1,400,000 water particles, respectively. In the large bilayer, the water amount was increased to ~3,700,000 particles at pulling forces of 100 and 200 kJ/mol nm to increase the box size in the direction normal to the bilayer plane.

For nonbonded interactions, we used the standard cutoffs for the MARTINI force field: the Lennard-Jones potential was shifted to zero between 0.9 and 1.2 nm, and the Coulomb potential was shifted to zero between 0 and 1.2 nm with a relative dielectric constant of 15. The time step was 20 fs with neighbor list updates every 10 steps. Lipids and water were coupled separately to a target temperature using the velocity rescaling thermostat (30) with a time constant of 1 ps. The system was coupled to normal and lateral pressures of 1 bar with a semi-isotropic pressure coupling scheme to provide a tensionless bilayer, or to a surface tension with a surface tension coupling scheme, in both cases using a Berendsen barostat (31) with a time constant of 4 ps and compressibility of 5 10^{-5} bar^{-1}. The simulation time was 2 μs for small systems and 1 μs for large systems. A summary of all simulations is given in Table 1.

Submitted January 24, 2012, and accepted for publication March 22, 2012.

*Correspondence: tieleman@ucalgary.ca

Editor: Scott Feller.

0006-3495/12/04/1866/6 $2.00

doi: 10.1016/j.bpj.2012.03.048

TABLE 1 Summary of the simulations performed

No. of lipids	Extraction conditions r_0* [nm]	f [kJ/mol·nm]	γ [mN/m]	Result	Tether parameters r [nm]	L_{max} [nm]	dL/dt [nm/ns]
4608	3	10		B			
		50		P		14	
		100		T	6.9	26	0.03
		150		T	6.0	34	0.06
		200		T	5.0	41	0.1
		225		R			
		200	10	P		11	
		200	2	T	4.8	39	
		200	−1	T	5.1	46	0.3
	4	100		T	7.4	28	0.02
		200		C	5.3	40	0.06
		300		R			
	5	100		T	7.5	26	0.01
		200		C	5.9	44	0.06
		300		R			
18,432	3	1		B			
		10		P		12	
		50		T	8.3	40	0.04
		100		T	6.1	60	0.2
		200		T	5.0	>87†	0.5
	—		−1	F			
			−6	F			
	30		−4	T	12	26	
			−6	T	13	28	
	40		−4	T	17	36	
			−6	T	20	40	

Here B is bilayer bending, P is protrusion, T is tether, R is rupture, C is catenoid-shaped tether, F is bilayer folding (see text for details), r_0 is the radius of the lipid patch to which the pulling force is applied, f is the magnitude of the pulling force, and γ is the surface tension in the bilayer.

*Pulling force simulations: radius of the lipid patch to which external force is applied (with lipids restrained in lateral direction). Lateral compression simulations: radius of unrestrained patch (with restraints in the normal direction applied to the remaining lipids).

†Further tether elongation was not possible due to the finite system size in the direction normal to the bilayer.

In simulations with an external pulling force, the center of mass of a lipid path of radius 3, 4, or 5 nm was pulled with a linear potential, resulting in a constant force. The lipids belonging to the patch were determined in the starting configuration. Position restraints in the lateral directions (x and y) were applied to the phosphate group of these lipids to keep them in the patch and prevent them from diffusing back into the bilayer. In the lateral compression simulations, position restraints in the normal direction were applied to phosphate groups of lipids at the bilayer perimeter, i.e., outside of a lipid patch of either 30 or 40 nm in radius, to prevent bilayer folding.

Tether diameters were calculated from the positions of the phosphate groups of lipids in the upper bilayer leaflet constituting the outer leaflet of the tether. We calculated the tether average radius (Table 1) considering only the part of the tether that adopts a cylindrical shape, i.e., disregarding the tip and the connection to the bilayer. The tether length was estimated from the maximum and minimum z-coordinates of the phosphate groups of lipids in the outer leaflet of the tether. Lipid flip-flop between the leaflets, given its low rate and the relatively short simulation times compared with typical flip-flop rates, was not taken into account in the calculation of the relative area strain between the leaflets and the nonlocal bending energy.

RESULTS AND DISCUSSION

Tethers were extracted from lipid bilayers by application of an external pulling force or by lateral compression. A summary of the simulations performed and their results is presented in Table 1. Tether formation was defined as bilayer deformation into a cylindrical shape (as opposed to bilayer bending and cone-shaped protrusions). Earlier simulations used preformed bilayer cylinders to calculate the bilayer bending modulus (32).

In the external force simulations, a constant force was exerted on the center of mass of a lipid patch in the direction normal to the bilayer plane. Coordinates of the phosphate groups of lipids in the patch were restrained in the lateral direction, modeling adhesion to a bead in experiments. Periodic boundary conditions in the lateral direction combined with the center-of-mass motion removal prevented normal displacement of the bilayer perimeter. A tether pulled from the large bilayer (80×80 nm^2) is shown in Fig. 1, *a* and *b*. The tether geometry resembles a small nanotube: a narrow water channel is surrounded by a cylindrically curved bilayer of nearly constant diameter, widening at its connection to the membrane.

Tether development is illustrated in Fig. 1, *c–e*, for the small patch (40×40 nm^2) under forces of different magnitude. A cone-shaped protrusion (Fig. 1 *c*) transformed into a cylindrical tube (Fig. 1 *d*), which grew in length (Fig. 1 *e*). Tether formation proceeded through these steps under strong pulling forces (cf. Table 1). Under weak pulling

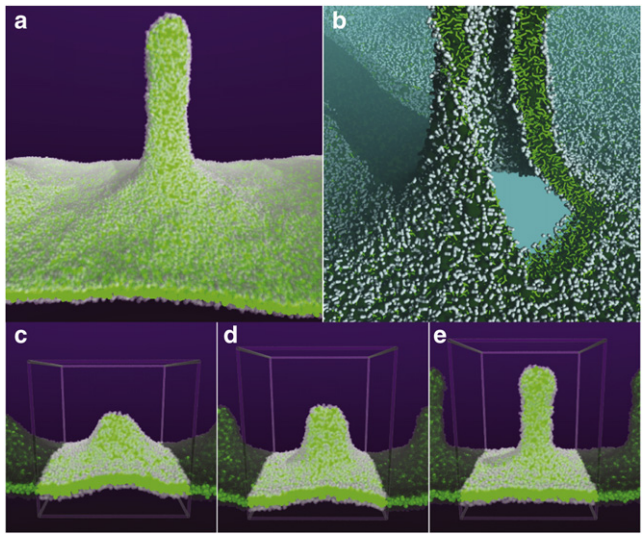

FIGURE 1 Tether pulled by external force, shown in side (*a*) and cross-section (*b*) views. The tether is produced by a force of 100 kJ/mol nm acting on lipid patch of radius 3 nm in a DOPC bilayer of 18,432 lipids. Steps of tether development: initial cone-shaped protrusion (*c*) transforms into a tube of constant diameter (*d*), which grows in length (*e*). Snapshots correspond to a force of 50, 100, and 200 kJ/mol nm, respectively, applied to a patch of radius 3 nm in a bilayer of 4608 DOPC. Violet, water; gray beads, lipid polar groups; green sticks, lipid apolar groups. The simulation box is highlighted in the bottom row.

forces, only an initial protrusion formed. Even larger forces led to tube rupture, which was initiated by local thinning of its diameter (Fig. 2). The mechanism of rupture was similar to fission of liposomes (33).

The evolution of the tether radius profile as a function of time is shown in Fig. 3 *a*. When the pulling force acted on larger lipid patches, the tube tip became wider than the tube diameter. This led to a theoretically predicted (34) catenoid-like shape (resembling the interior of a torus). This shape here is likely an artifact related to high pulling rates, because at lower pulling rates (in a larger bilayer) a cylindrical tube of a larger radius would be produced.

Theoretical models have described tether development as a two-step process including initial viscoelastic deformation of the membrane followed by viscous flow of lipids into the tube (35,36). The crossover between these two phases of tether development takes place for pulling forces above a threshold. In our simulations, we were able to reproduce this behavior. In Fig. 3 *b*, tether development under a constant pulling force is shown. A crossover from a protrusion to a growing tether regime manifests as a change in slope in tether elongation versus time. The threshold force depended on the size of the bilayer, decreasing with increasing system size. Tether growth was linear at a constant applied force, in agreement with theoretical predictions (36). Tube linear elongation was always limited by the finite bilayer size in the simulation. Tether formation was also reversible: reduction or removal of the external force resulted in tether retraction or complete respreading. Application of a positive surface tension to the bilayer in combination with a pulling force led to a reduction in the tether diameter, as expected, or, at higher magnitudes, prevented the transformation from protrusion to tether. Negative surface tension (i.e., bilayer compression), in turn, facilitated the flow of lipids into the tether.

Experimental studies (17,18) have shown that tethers can be formed by lateral compression of the membrane alone, i.e., without pulling. To mimic this in simulations, we applied a negative surface tension to large bilayers with position restraints at the perimeter to prevent bilayer folding (see Table 1). Bilayer folding was similar to monolayer folding (37) and resulted from bilayer bending in one direction (lowering the bending energy) and formation of a periodic stack of four leaflets perpendicular to the bilayer plane. Position restraints may model confinement of the bilayer by the presence of molecules such as polymers in surrounding solution, or attachment of the membrane to the cytoskeleton. Tube development started from undulations of the unrestrained bilayer area (Fig. 4 *a*), and resulted in a short tube of a wider diameter of ~30 nm (Fig. 4 *b*). In agreement with theoretical predictions (18), these tethers had unfavorable bending energy (at zero spontaneous curvature of the DOPC bilayer). The tethers slowly retracted via diffusion of unrestrained lipids back into the bilayer, simultaneously increasing its undulations; however, we were able to prevent retraction by keeping the area of the compressed bilayer constant.

From the tether-pulling simulations we can extract material properties of the membrane, including the bending

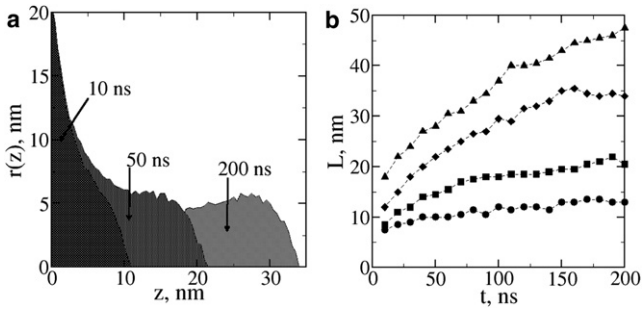

FIGURE 3 Tether development under constant pulling force. (*a*) Distribution of the tether radius along its axis as a function of time. A force of 200 kJ/mol nm is acting on a lipid patch of radius 3 nm in a DOPC bilayer of 4608 lipids. The radius is determined using the coordinates of the phosphate groups in the outer leaflet. (*b*) Tether elongation as a function of time is shown for forces of 50 (*circles*), 100 (*squares* and *triangles*), and 200 (*diamonds*) kJ/mol nm acting on a patch of radius 3 nm in a DOPC bilayer of 4608 or 18,432 (*triangles*) lipids. The force of 50 kJ/mol nm is below the threshold, and the crossover from protrusion to tether does not occur (see text for details).

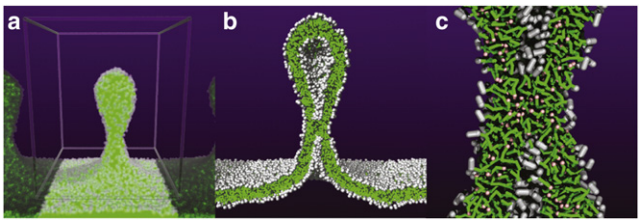

FIGURE 2 Tether rupture by a strong pulling force, shown in side (*a*), cross-section (*b*), and close-up (*c*) views. A force of 300 kJ/mol nm is acting on lipid patch of radius 4 nm in a DOPC bilayer of 4608 lipids. Color scheme as in Fig. 1; lipid tail ends are shown as pink spheres in panel *c*.

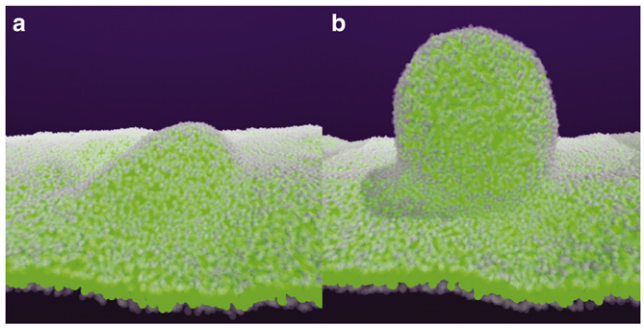

FIGURE 4 Tether formation under lateral compression. Undulations of unrestrained bilayer area (*a*) are followed by the formation of a wider tether (*b*). A negative surface tension of −4 mN/m is acting on a bilayer of 18432 DOPC lipids. Position restraints are applied to prevent normal displacement of the lipids at the bilayer perimeter (unrestrained patch radius is 40 nm). Color scheme as in Fig. 1.

modulus, viscosity, and tether tension. Static forces that counteract tether elongation originate from local and nonlocal bending energies associated with bilayer deformation. The local bending energy arises from elastic resistance of the bilayer to curvature as it is pulled into a tube. The nonlocal bending energy accounts for the curvature-induced relative strain between the leaflets of the closed bilayer (containing a fixed number of lipids) (19,38). Using the Helfrich Hamiltonian (39), the local bending energy reads $E_b = \pi K_b L/r$, where K_b is the bilayer bending modulus, r is the tether radius, and L is the tether length. Nonlocal bending energy is given by (19,38) $E_r = K_r \Delta A^2/(2A_0 h^2)$, where $\Delta A = 2\pi Lh$ is the relative area difference between the inner and outer bilayer leaflets in the tube, K_r is the nonlocal bending modulus, h is the distance between the neutral surfaces of each leaflet, and A_0 is the total bilayer area. It is worth noting that although the area of cells and artificial liposomes (~1–100 μm^2) is large compared with the area incorporated in the tether, its small value in our simulations (~40 × 40 or 80 × 80 nm^2 for the two considered bilayer sizes) increases the contribution of this term to the tether energy by several orders of magnitude. The dependence of this term on the bilayer area leads to the observed decrease of the threshold force with increasing size of the simulated system (cf. Table 1). The nonlocal bending term, which increases with tether length due to an increase in the relative area difference between the leaflets, also explains the limited linear tether growth at a constant force in our simulations.

The tether force, which arises from both local and nonlocal bending, is given by $f = 2\pi K_b/r + 4\pi^2 K_r L/A_0$. Using a typical ratio (19,40) of K_r/K_b~3, at a pulling force of 100 kJ/mol nm and a patch radius of 3 nm, we obtain a bending modulus K_b~1 × 10^{-19} J. The value is similar for the small and large bilayers in a range of pulling forces (cf. Table 2). A slight increase in the apparent K_b value with increasing force likely originates from higher viscous dissipation resulting in higher dynamic forces (at higher pulling speeds). To calculate K_b, we used the tether length at the transition point between protrusion formation and the beginning of the linear growth regime. The obtained estimates are in good agreement with the experimentally measured value of 0.9 10^{-19} J (41) and previous simulation result of 0.6 10^{-19} J (42) for DOPC bilayers. Recent studies, however, reported somewhat higher bending moduli for bilayers in the MARTINI force field (43,44). Our value of the bending modulus may be somewhat overestimated due to the small radius of the tubes, leading to a possible coupling between the bending and area stretching deformations not accounted for in the above formulas.

The surface tension in the tether, γ_t, can then be obtained with the following formula (19,22): $r = \sqrt{K_b/2\gamma_t}$. Using the above estimates, we find a surface tension in the tether of ~1 mN/m, which is larger than the surface tension in the tensionless bilayer, in agreement with theoretical predictions (38). Note that the calculated bending modulus and the surface tension in the tether increase with increasing pulling rate. This is because the tether pulling forces used in the estimates of these properties contain both static and viscous friction contributions. Viscous dissipation in turn increases with an increasing pulling rate.

TABLE 2 Bilayer material properties calculated from tethers pulled by external force

No. of lipids	r_0 [nm]	f [kJ/mol nm]	L_0 [nm]	$K_b \cdot 10^{20}$ [J]	γ_t [mN/m]	f_0 [kJ/mol nm]	$\eta_{eff} \cdot 10^{10}$ [Pa·m·s]
4608	3	100	17	9	0.9	60	24
		150	19	11	1.6		
		200	22	13	2.5		
18,432	3	50	25	7	0.5	36	5
		100	22	12	1.7		
		200	24	20	4.2		

Here r_0 is the radius of the patch to which the pulling force is applied; f is the magnitude of the pulling force; L_0 is the tether length at the end of the protrusion formation, which is followed by linear growth; K_b is the bending modulus of the bilayer; γ_t is the surface tension in the tether; f_0 is the tether force at zero velocity; and η_{eff} is the effective surface viscosity.

The tether force that arises from viscous friction comprises the bilayer surface flow, mutual slide of the leaflets, and drag of the associated solvent (22,23,45). Viscous friction can be assessed by calculating the effective surface viscosity in the system. This effective surface viscosity represents an apparent bulk viscosity multiplied by a characteristic length, which is equal to the thickness of the bilayer and the associated solvent layers. To quantify this, we can assume a simple linear force-velocity relationship, $f = f_0 + \eta_{eff} dL/dt$(22), where the effective surface viscosity η_{eff} does not depend on the tether elongation rate dL/dt. We can then estimate the effective surface viscosity η_{eff} and the force at zero velocity, f_0, by fitting this linear relationship to the force versus growth rate data (cf. Table 2). Of interest, the calculated static forces are close to the threshold forces in our simulations. This explains why lower pulling forces did not produce tethers in our simulations. The calculated effective surface viscosities, ~1 × 10^{-9} Pa·m·s, are in good agreement with experimental data for model bilayers (22,23). Note that the calculated values decrease with increasing size of the simulated system. This could result from confinement of the associated solvent, which has been shown to increase the apparent solvent viscosity (46). Using the estimate for the bilayer surface viscosity $\eta_b \sim G(s)/s$ with the shear modulus $G(s)$ at the pulling rate s~0.1 nm/ns from Baoukina et al. (37), we expect the contribution of bilayer surface flow to the effective viscosity to be relatively small at ~1 × 10^{-10} Pa·m·s. On the basis of the combined results, we find that the contributions of static and viscous forces to the total tether force are comparable.

In our simulations, several conditions are distinct from pulling cellular tethers in experiments. Cellular membranes

are typically attached to the underlying cytoskeleton; adhesion to the cytoskeleton contributes to the static force, and the flow of lipids through the cytoskeleton network leads to viscous dissipation (22,23,45,47). The crossover from a protrusion to tether elongation typically occurs when the membrane separates from the underlying cytoskeleton. In our model membranes, adhesion is not included in the pulling force simulations, and processes of a different nature contribute to both dynamic and static forces. Despite these differences, it is worthwhile to compare the tether extraction parameters in our simulations with experimental conditions. The forces that lead to tether growth in simulations (~100 pN) are one to two orders of magnitude larger than experimental values. At the same time, the tether radii lie at the lower limit (~10 nm) of the experimental values. Larger forces result in faster pulling rates, which in the simulations are at least two orders of magnitude higher than those used experimentally for model membranes ($\sim 10^{-4}$ m/s) (23). At comparable effective viscosities, faster rates lead to higher viscous forces. On the other hand, the static forces in the simulations are also larger than experimental ones due to the much smaller membrane size. The latter limits the scale of tether-induced deformation and thus leads to higher nonlocal bending energy, coupling between the bending and stretching deformations, and curvature dependence of the elastic moduli (48).

In summary, using molecular dynamics simulations, we reproduced tether formation from model membranes under applied external force as well as lateral compression. These simulations gave detailed structural information on tethers and tether formation, and provide a link between molecular simulation and membrane material properties.

This work was supported by the Natural Sciences and Engineering Research Council (Canada). D.P.T. is an Alberta Innovates Health Solutions Scientist. The simulations were performed on Westgrid/Compute Canada facilities.

REFERENCES

1. Lee, C., and L. B. Chen. 1988. Dynamic behavior of endoplasmic reticulum in living cells. *Cell.* 54:37–46.
2. Benard, G., and R. Rossignol. 2008. Ultrastructure of the mitochondrion and its bearing on function and bioenergetics. *Antioxid. Redox Signal.* 10:1313–1342.
3. De Matteis, M. A., and A. Luini. 2008. Exiting the Golgi complex. *Nat. Rev. Mol. Cell Biol.* 9:273–284.
4. Maxfield, F. R., and T. E. McGraw. 2004. Endocytic recycling. *Nat. Rev. Mol. Cell Biol.* 5:121–132.
5. Shibata, Y., G. K. Voeltz, and T. A. Rapoport. 2006. Rough sheets and smooth tubules. *Cell.* 126:435–439.
6. Rustom, A., R. Saffrich, …, H. H. Gerdes. 2004. Nanotubular highways for intercellular organelle transport. *Science.* 303:1007–1010.
7. White, J., L. Johannes, …, E. H. Stelzer. 1999. Rab6 coordinates a novel Golgi to ER retrograde transport pathway in live cells. *J. Cell Biol.* 147:743–760.
8. Davis, D. M., and S. Sowinski. 2008. Membrane nanotubes: dynamic long-distance connections between animal cells. *Nat. Rev. Mol. Cell Biol.* 9:431–436.
9. Leduc, C., O. Campàs, …, P. Bassereau. 2010. Mechanism of membrane nanotube formation by molecular motors. *Biochim. Biophys. Acta.* 1798:1418–1426.
10. Leduc, C., O. Campàs, …, J. Prost. 2004. Cooperative extraction of membrane nanotubes by molecular motors. *Proc. Natl. Acad. Sci. USA.* 101:17096–17101.
11. Shao, J. Y., and R. M. Hochmuth. 1996. Micropipette suction for measuring piconewton forces of adhesion and tether formation from neutrophil membranes. *Biophys. J.* 71:2892–2901.
12. Waugh, R. E. 1982. Surface viscosity measurements from large bilayer vesicle tether formation. 2. Experiments. *Biophys. J.* 38:29–37.
13. Hochmuth, R. M., N. Mohandas, and P. L. Blackshear, Jr. 1973. Measurement of the elastic modulus for red cell membrane using a fluid mechanical technique. *Biophys. J.* 13:747–762.
14. Bo, L., and R. E. Waugh. 1989. Determination of bilayer membrane bending stiffness by tether formation from giant, thin-walled vesicles. *Biophys. J.* 55:509–517.
15. Hochmuth, R. M., H. C. Wiles, …, J. T. McCown. 1982. Extensional flow of erythrocyte-membrane from cell body to elastic tether. 2. Experiment. *Biophys. J.* 39:83–89.
16. Hosu, B. G., M. Sun, …, G. Forgacs. 2007. Eukaryotic membrane tethers revisited using magnetic tweezers. *Phys. Biol.* 4:67–78.
17. Staykova, M., D. P. Holmes, …, H. A. Stone. 2011. Mechanics of surface area regulation in cells examined with confined lipid membranes. *Proc. Natl. Acad. Sci. USA.* 108:9084–9088.
18. Li, Y. H., R. Lipowsky, and R. Dimova. 2011. Membrane nanotubes induced by aqueous phase separation and stabilized by spontaneous curvature. *Proc. Natl. Acad. Sci. USA.* 108:4731–4736.
19. Waugh, R. E., J. Song, …, B. Zeks. 1992. Local and nonlocal curvature elasticity in bilayer membranes by tether formation from lecithin vesicles. *Biophys. J.* 61:974–982.
20. Borghi, N., and F. Brochard-Wyart. 2007. Tether extrusion from red blood cells: integral proteins unbinding from cytoskeleton. *Biophys. J.* 93:1369–1379.
21. Waugh, R. E., and R. M. Hochmuth. 1987. Mechanical equilibrium of thick, hollow, liquid membrane cylinders. *Biophys. J.* 52:391–400.
22. Hochmuth, F. M., J. Y. Shao, …, M. P. Sheetz. 1996. Deformation and flow of membrane into tethers extracted from neuronal growth cones. *Biophys. J.* 70:358–369.
23. Evans, E., and A. Yeung. 1994. Hidden dynamics in rapid changes of bilayer shape. *Chem. Phys. Lipids.* 73:39–56.
24. Derényi, I., F. Jülicher, and J. Prost. 2002. Formation and interaction of membrane tubes. *Phys. Rev. Lett.* 88:238101.
25. Sorre, B., A. Callan-Jones, …, P. Bassereau. 2009. Curvature-driven lipid sorting needs proximity to a demixing point and is aided by proteins. *Proc. Natl. Acad. Sci. USA.* 106:5622–5626.
26. Tian, A., and T. Baumgart. 2009. Sorting of lipids and proteins in membrane curvature gradients. *Biophys. J.* 96:2676–2688.
27. Marrink, S. J., H. J. Risselada, …, A. H. de Vries. 2007. The MARTINI force field: coarse grained model for biomolecular simulations. *J. Phys. Chem. B.* 111:7812–7824.
28. Marrink, S. J., A. H. de Vries, and D. P. Tieleman. 2009. Lipids on the move: simulations of membrane pores, domains, stalks and curves. *Biochim. Biophys. Acta.* 1788:149–168.
29. Hess, B., C. Kutzner, …, E. Lindahl. 2008. GROMACS 4: algorithms for highly efficient, load-balanced, and scalable molecular simulation. *J. Chem. Theory Comput.* 4:435–447.
30. Bussi, G., D. Donadio, and M. Parrinello. 2007. Canonical sampling through velocity rescaling. *J. Chem. Phys.* 126:014101.
31. Berendsen, H. J. C., J. P. M. Postma, …, J. R. Haak. 1984. Molecular dynamics with coupling to an external bath. *J. Chem. Phys.* 81:3684–3690.

32. Harmandaris, V. A., and M. Deserno. 2006. A novel method for measuring the bending rigidity of model lipid membranes by simulating tethers. *J. Chem. Phys.* 125:204905.

33. Markvoort, A. J., and S. J. Marrink. 2011. Lipid acrobatics in the membrane fusion arena. *Curr. Top Membr.* 68:259–294.

34. Powers, T. R., G. Huber, and R. E. Goldstein. 2002. Fluid-membrane tethers: minimal surfaces and elastic boundary layers. *Phys. Rev. E.* 65:041901.

35. Nowak, S. A., and T. Chou. 2010. Models of dynamic extraction of lipid tethers from cell membranes. *Phys. Biol.* 7:026002.

36. Pospieszalska, M. K., I. Lasiecka, and K. Ley. 2011. Cell protrusions and tethers: a unified approach. *Biophys. J.* 100:1697–1707.

37. Baoukina, S., L. Monticelli, …, D. P. Tieleman. 2008. The molecular mechanism of lipid monolayer collapse. *Proc. Natl. Acad. Sci. USA.* 105:10803–10808.

38. Glassinger, E., and R. M. Raphael. 2006. Influence of thermally driven surface undulations on tethers formed from bilayer membranes. *Biophys. J.* 91:619–625.

39. Helfrich, W. 1973. Elastic properties of lipid bilayers: theory and possible experiments. *Z. Naturforsch. C.* 28(11, C):693–703.

40. Raphael, R. M., and R. E. Waugh. 1996. Accelerated interleaflet transport of phosphatidylcholine molecules in membranes under deformation. *Biophys. J.* 71:1374–1388.

41. Rawicz, W., K. C. Olbrich, …, E. Evans. 2000. Effect of chain length and unsaturation on elasticity of lipid bilayers. *Biophys. J.* 79:328–339.

42. Wong-Ekkabut, J., S. Baoukina, …, L. Monticelli. 2008. Computer simulation study of fullerene translocation through lipid membranes. *Nat. Nanotechnol.* 3:363–368.

43. Brandt, E. G., A. R. Braun, …, O. Edholm. 2011. Interpretation of fluctuation spectra in lipid bilayer simulations. *Biophys. J.* 100:2104–2111.

44. Watson, M. C., E. S. Penev, …, F. L. Brown. 2011. Thermal fluctuations in shape, thickness, and molecular orientation in lipid bilayers. *J. Chem. Phys.* 135:244701.

45. Brochard-Wyart, F., N. Borghi, …, P. Nassoy. 2006. Hydrodynamic narrowing of tubes extruded from cells. *Proc. Natl. Acad. Sci. USA.* 103:7660–7663.

46. Gov, N., A. G. Zilman, and S. Safran. 2004. Hydrodynamics of confined membranes. *Phys. Rev. E.* 70:011104.

47. Heinrich, V., A. Leung, and E. Evans. 2005. Nano- to microscale dynamics of P-selectin detachment from leukocyte interfaces. II. Tether flow terminated by P-selectin dissociation from PSGL-1. *Biophys. J.* 88:2299–2308.

48. Risselada, H. J., S. J. Marrink, and M. Müller. 2011. Curvature-dependent elastic properties of liquid-ordered domains result in inverted domain sorting on uniaxially compressed vesicles. *Phys. Rev. Lett.* 106:148102.